Photocatalytic activity of ZnO nanoparticles towards tinidazole degradation: Experimental design by response surface methodology (RSM)

Leila Daneshvar, Alireza Nezamzadeh-Ejhieh*

Department of Chemistry, Shahreza Branch, Islamic Azad University, P.O. Box 311-86145, Shahreza, Isfahan, Iran, Tel. +98 31-53292515, Fax +98 31-53291018, email: arnezamzadeh@iaush.ac.ir (A. Nezamzadeh-Ejhieh)

ABSTRACT

In this work, ZnO nanoparticles (ZnO-NPS) were synthesized, characterized and used in photo catalytic degradation of tinidazole (TNZ) aqueous solution. A medium pressure Hg lamp (35 W) was used as radiation source. To study the interactions between the key operating parameters, the experiments were designed by using response surface methodology (RSM). The best run to achieve the maximum response was included C_{TNZ}: 2.5 mg/L at pH 6.3, 0.76 g/L of ZnO and irradiation time of 90 min. To confirm the degradation extent of TNZ, HPLC and COD were used. Based on HPLC and COD results 62% and 70% of TNZ molecules have degraded during 90 min photo degradation of sample, respectively.

Keywords: ZnO; Photo degradation; Tinidazole; Nano-particles; RSM; Experimental design

1. Introduction

Nowadays, high pharmaceutical consumption by human has led to presence of high level of pharmaceutical compounds in the aquatic environment. Antibiotics are one the most common pharmaceutical water pollutants. Some of these water pollutants, with high toxicity, cannot be easily biodegraded. Hence, their presence in water causes to mutagenic and carcinogenic effects [1–4]. Unfortunately, traditional wastewater treatment techniques cannot completely remove many antibiotics from the treated wastewater samples. Hence, discharging of such wastewater to the environment causes there leasing of a high level of antibiotics into surface water. This causes the antibiotics in the surface water to be present at higher amounts of the allowed dosages. In general, long exposure to low dosages of antibiotics causes the induction of resistance in bacterial strains. Finally, transferring of this resistance to humans via environmental exposure causes serious problems in body life. Such organic compounds have complex molecular structure and hence the conventional biological process cannot adequately remove them from water/ wastewater samples [5]. In general, the most effective techniques for the removal of different organic pollutants are advanced oxidation processes (AOPs) based on the production of powerful oxidants such as hydroxyl and super oxide radicals [6,7].

In semi conducting based photo catalysis excitation of a semi conducting material, such as transition metal sulfides or oxides, by suitable photon energy provides electron and hole (e/h) pairs in its conduction and valence bands, respectively. The resulted e/h pairs act as active centers for reaction with dissolved oxygen and water molecules/ hydroxyl anions to produce super oxide and hydroxyl radicals, respectively. These powerful oxidants ($E°$: $^•OH/OH^- = 2.27V$, $^•OH/H_2O = 2.38$ V) can rapidly and non-selectively attack to organic pollutants are present in the media and cleavage them to smaller fragments. The produced holes can also directly attack to organic matters in the solution and brake them. Final goal of heterogeneous photo catalytic degradation (or other AOP methods) is mineralizing of the organic matters to water and carbon dioxide molecules [8–17]. One of the most important limiting factors in heterogeneous photo catalysis is recombination of e/h pairs which significantly decreases the degradation efficiency. One strategy for diminishing of this drawback is using of semiconductors nanoparticles. These materials have high effective

*Corresponding author.

surface area which reduces the path length for rapid migration of photo generated electrons to the surface of the catalysts before they can combine with the generated holes. High effective surface area of nanoparticles adsorb high amount of the pollutant at the catalyst surface, where hydroxyl radicals produced. Hydroxyl radicals have very short life time about a few nanosecond and they should immediately react with pollutant molecules [18]. Hence, the produced radicals immediately degrade the adsorbed pollutants on the surface of semiconductors nanoparticles [19,20].

ZnO, with a direct band gap of 3.3 eV, has unique physico chemical properties, long term photo stability with respect to many metal oxides, environmental stability, strong oxidizing power and non-toxicity. Hence, it has been widely used in semi conducting based photo catalysis processes [21–31]. The most important advantage of ZnO is its capability to absorb in over a larger fraction of the UV–Vis spectrum with respect to titanium dioxide [32].

In this work a simple method was used for the synthesis of ZnO nanoparticles (NPs) and the as synthesized ZnO-NPs were then used in photo degradation of tinidazole (TNZ) aqueous solution. Tinidazole (a derivative of 2-methylimidazole and a prominent member of the nitroimidazole antibiotics) as an anti-parasitic drug can use against protozoan infections (for a variety of amoebic and parasitic infections. It has some side effects. Drinking alcohol while taking tinidazole can cause an unpleasant disulfiram-like reaction, which includes nausea, vomiting, headache, increased blood pressure, flushing, and shortness of breath [33].

The work focused on the study the interaction effects between the influencing factors on the degradation extent of the pollutant. Hence, the experiments were designed by response surface methodology (RSM). In spite of the 'one factor at a time (OFAT)' as common method for analytical chemists, RSM provides much informations about the interaction effects of the parameters. It also decreases the numbers of needed experiments for performing a research work [34].
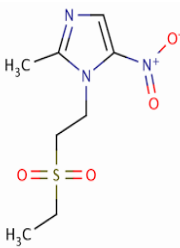
For synthesis of ZnO-NPs, 4 g of zinc nitrate and 2.99 g of glycine was added to a 50 mL porcelain crucible and mixed thoroughly. Then, exactly 15 mL of water was added and pH of the solution was adjusted at 6 by adding ammonia. The content of the crucible was magnetically shaken for 7 h while it was located in a water bath at 60°C. Then, the resulted gel was placed on a flame for auto combustion. Finally, the resulted material was calcined at 600°C for 2 h [35]. In general, capping agent/surfactant/stabilizing agent plays an important role for prevent uncontrollable growth of particles and particle aggregation, also controls growth rate and particle size. It also allows particle solubility in different solvents. All the mentioned parameters can be achieved by electrostatic stabilization. On the other hand, when metal ions adsorbed on the surface, an electrical double layer can form which results in a Columbic repulsion force between individual particles and prevent from aggregation of NPs. Also, in steric stabilization, the metal center can be surrounded by layers of material that are sterically bulky. Hence, these bulky species cannot be aggregated. Here, glycine plays such roles. It has an iso-electric point at pH 6 which in this point it is present as dipole-ion species as predominant species. In this case, it can complex Zn(II) cations from its negative head group, and the positively charged head groups are present at the opposite head. These positively charged head groups repel the resulted species and prevent from their aggregation.

For preparation of tinidazole solution, the content of a 500 mg capsule (Kimia Ara Co., IRAN, with total powder weight of 6710 mg) was thoroughly mixed and 134 mg of the powder was dissolved in water and shaken for 30 min for complete dissolution. The resulted solution was diluted to 100 mL in a volumetric flask. This stock solution (with concentration about 1000 mg L^{-1} TNZ) was used for preparation of much diluter solutions via serial dilution method. Some chemical information of tinidazole are summarized in Table 1.

2. Experimental

2.1. Reagents and preparations

All reagent used with analytical grade purity were purchased from Merck or Aldrich. Distilled water was used for preparation of the solutions.

2.2. Catalyst characterization

The as-synthesized ZnO-NPs were characterized by the following instruments. X-ray diffractometer (Bruker, D8AD-VANCE,Germany, X-ray tube anode: Cu, wavelength: 1.5406 Å (Cu Kα), filter: Ni); Infrared spectrometer (Nicollet single beam FT-IR Impact400D); Scanning electron microscope

Table 1
Some chemical information of tinidazole

Structure	Formula	Trade names	Acidity	Solubility
	$C_8H_{13}N_3O_4S$ MW: 247.273 g/mol	Fasigyn, Simplotan, Tindamax	pKa: 3.1	19.9 g/L in water

(SEM, Philips XL30); UV–Vis spectrophotometer (Carry100, Australia); Brunauer-Emmett-Teller (BET, F12).

2.3. The photo catalytic degradation experiments

A 10 mL TNZ suspension (5 mg L^{-1} TNZ, 1 g L^{-1} ZnO NPs) was irradiated with a medium pressure Hg lamp (35 W, Philips, λ = 254 nm, 0.15 W/m^2, 60 cm length, Japan) located at 10 cm above the reactor, a cylindrical Pyrex-glass cell with 5 cm inside diameter and 10 cm height). After sampling at definite time intervals and centrifugation of the suspension (>13,000 rpm), absorbance of the cleaned solution was recorded at λ_{max} = 318. Using absorbance of the TNZ solutions before (A_o with C_o) and after irradiation at time t (A_t with C_t) the degradation extent of TNZ was estimated according to the following equation. The corresponding C/C_o values were also considered for these calculations. A schematic diagram for photo reactor is shown in FSD1 (see supplementary data).

$$TNZ \ \deg radiation\% = \left[\frac{(C_o - C_t)}{C_t}\right] \times 100 = \left[\frac{(A_o - A_t)}{A_t}\right] \times 100 \quad (1)$$

3. Results and discussion

3.1. Characterization

3.1.1. XRD pattern and FTIR spectrum

The X-ray diffraction (XRD) pattern of the as-synthesized ZnONPs is shown in Fig. 1A. All peaks were assigned based on their corresponding *hkl* planes for the wurtzite hexagonal phase of ZnO according to JCPDS 36-1451. This confirms production of high crystallite pure ZnO phase. Based on the Scherer equation [36], average crystallite size of ZnO NPs was estimated about 28 nm.

In the FT-IR spectrum of the ZnO-NPs in Fig. 1B, the broad absorption peak around 3416 cm^{-1} belongs to the normal polymeric O–H stretching vibration of H$_2$O. The located peak at 1633 cm^{-1} belongs to bending vibration of adsorbed water molecules onto ZnONPs. The absorption band at 1385 cm^{-1} may show the presence of C–O group that remained from the initial reactants. Nitrogen contained groups can

show absorption peaks around 2800 cm^{-1}. Overlapping of these peaks with the absorption peak of O–H stretching vibration at 3400 cm^{-1} caused to creation of a broad peak in this region [37–39]. The main peak of the Zn-O bond is present at 564 cm^{-1} for pure ZnO, reported also in literature [40].

3.1.2. Morphology and surface properties of ZnO-NPs

Typical SEM images (A,B) for the ZnO- NPs are shown in Fig. 2 which show that the morphology of ZnO includes cauliflower-like androd shapes. The images also show formation of nanoparticles for ZnO. X-ray mapping image is also shown in Fig. 2C, confirming well dispersion of Zn and O atoms through the ZnO structure. EDX spectrum of the sample in Fig. 2D confirms high purity of the as-synthesized sample.

The N$_2$ adsorption/desorption curve and the corresponding Brunauer–Emmett–Teller (BET) curve for the ZnO-NPs are shown in Fig. 3. This method was used to estimate the surface properties of the catalyst that play very important role in the catalytic activity. The BET surface area, pore volume, and pore diameter of ZnO were obtained about 11.14 m^2/g, 0.235 cm^3/g and 84.2 nm, respectively.

3.1.3. Diffuse reflectance spectra

For estimation of energy gap of the as synthesized NiO NPs, its optical absorption behavior was studied using UV–Vis diffuse reflectance spectroscopy (UV-Vis DRS). The obtained data were subjected by the following Kubelka-Munk equation, in which E_g is the semiconductors' band gap (eV), β is the absorption constant and α is the absorption coefficient defined by the Beer-Lambert's law as α = ([2.303×Abs]/d), ('d' is the sample thickness). The index 'n' has different values of 1/2, 2, 3/2, and 3 for allowed direct, allowed indirect, forbidden direct and forbidden indirect electronic transitions [41–43].

$$(\alpha h\nu) = \beta(h\nu - E_g)^n$$

To estimate the band gap energy, typical Tauc plot (($\alpha h\nu)^n$ – $h\nu$ curve) was drown for the allowed direct transi-
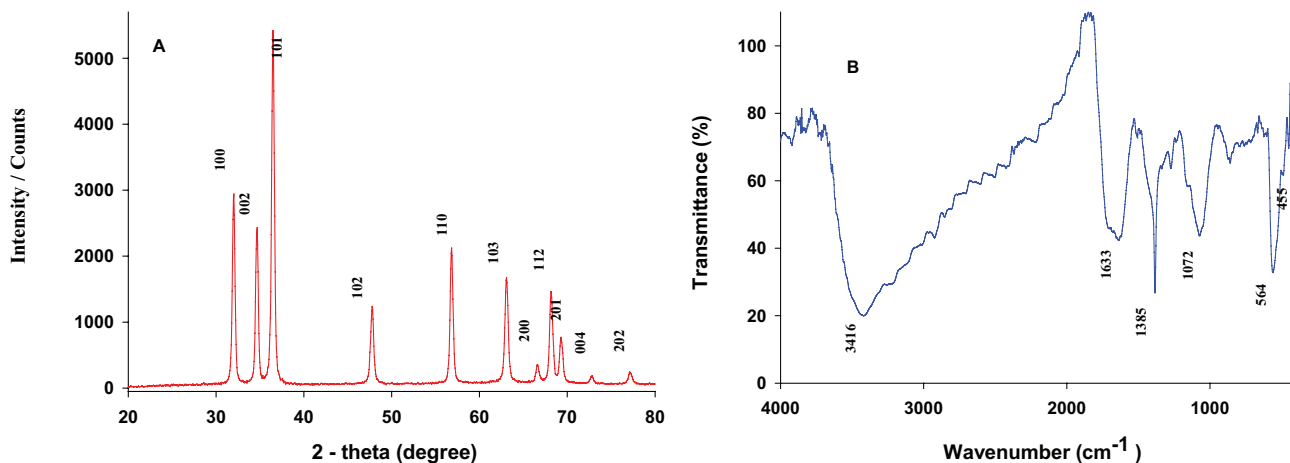

Fig. 1. XRD pattern (A) and FTIR spectrum (B) of as-synthesized ZnO NPs.
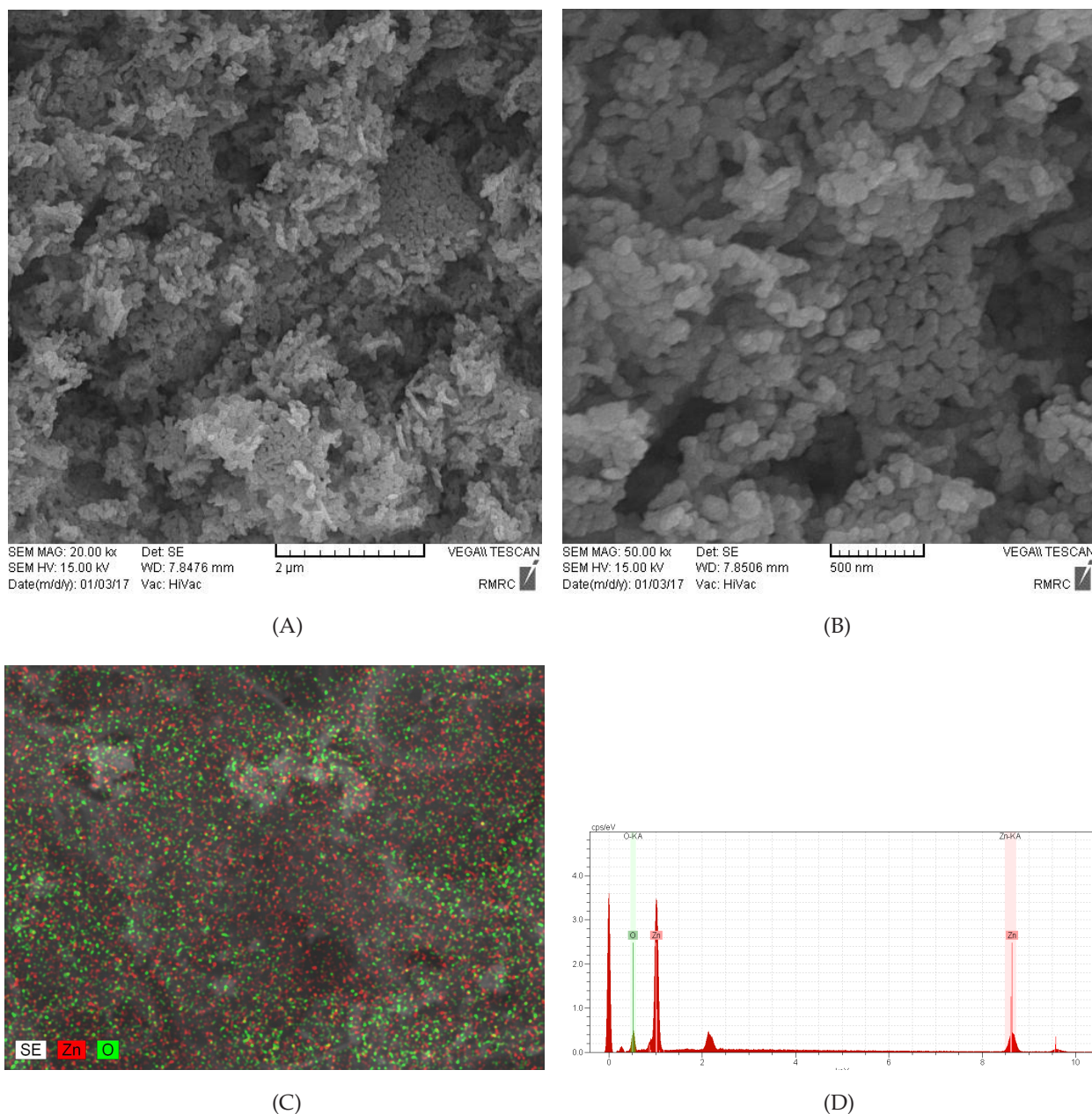
(A)

(B)

(C)

(D)

Fig. 2. SEM images (A,B), X-ray mapping image (C) and EDX spectrum (D) for the as-synthesized ZnO NPs.

tion and by extrapolation of the linear portion of the curve, the value of 3.39 eV was estimated (Fig. 3B). The value is relatively greater than the value of 3.3 eV for bulk ZnO, confirming formation of ZnO NPs in this work.

3.2. Preliminary photo catalytic experiments

As shown in Fig. 4A, surface adsorption and direct photolysis under Hg lamp irradiation have no considerable role in TNZ removal after 90 min. Hence, before all photo degradation experiments, all suspensions were shaken at dark for 20 min to reach equilibrium adsorption/desorption processes (surface adsorption remained constant after 15 min). Ability of ZnO NPs for the degradation of TNZ is confirmed in Fig.

4A at the applied conditions (C_{TNZ}: 5 mg/L at pH 6, 0.6 g/L of ZnO, irradiation time 90 min). Under these conditions, the C/C_o value of 0.46 correspond to degradation extent of 54% was obtained. Due to positive role of ZnO photo catalyst in the removal of TNZ, effect of calcination time on the activity of ZnO was studied. As shown in Fig. 4B, among the ZnO catalysts calcined at 600°C for 2, 4 and 6 h, the best activity was obtained for 2 h. At longer times, ZnO NPs may aggregate and effective surface area tends to decrease.

3.3. Experimental design (RSM) studies

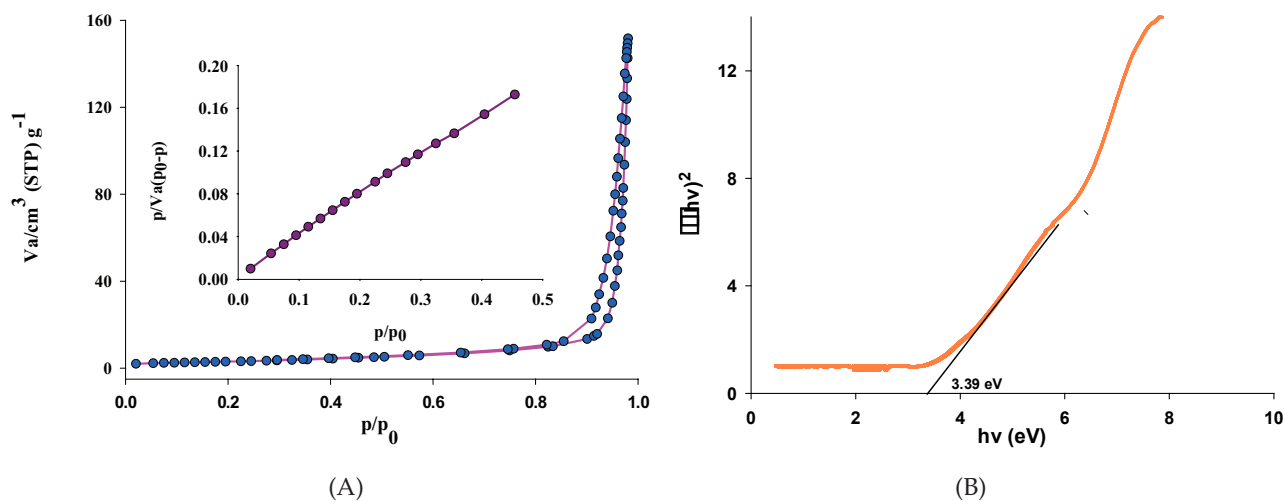Before construction a RSM matrix, screening of experimental variables was done to select the most important

Fig. 3. A) The N_2 adsorption/desorption isotherm at 77 K and the corresponding BET curve (inset) of ZnO-NPs; B) Typical Tauc plot obtained based on DRS spectrum of ZnO-NPs for estimation of its band gap energy.
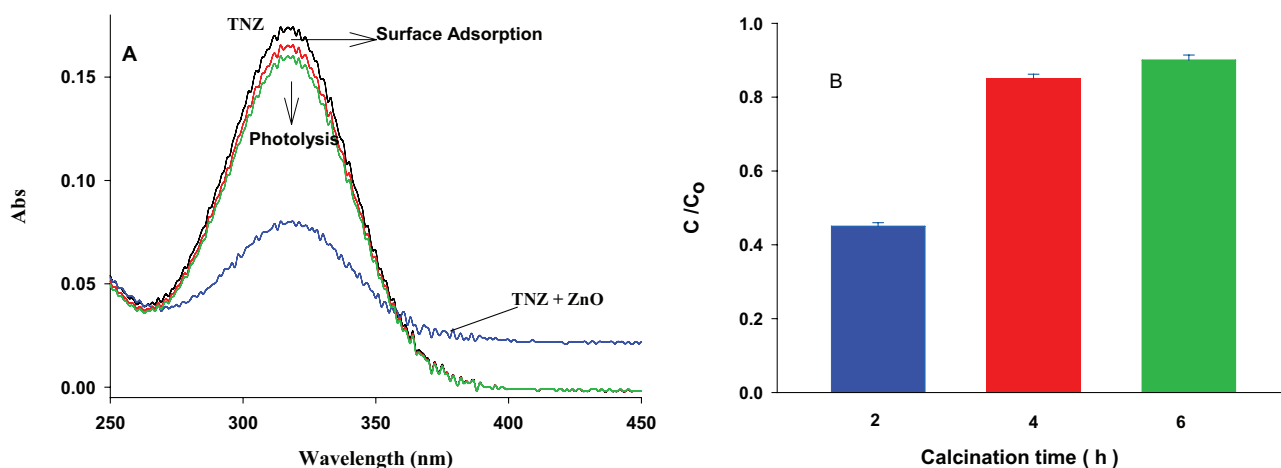

Fig. 4.(A) Effects of surface adsorption, direct photolysis and photocatalysis processes on the removal of TNZ, (C_{TNZ}: 5 mg/L at pH 6, 0.6 g/L of ZnO, irradiation time 90 min); (B) Effect of calcinations time on the activity of ZnO-NPs calcined at 600°C in photodegradation of TNZ at the above mentioned conditions (results averaged based on triplicate measurements).

influencing variables on the response (degradation extent of TNZ). For this goal all experimental variables including TNZ solution pH, C_{TNZ}, dose of ZnO NPs, calcination temperature used for ZnO preparation, irradiation time and intensity etc were used and the 'Plackett-Burman design' was applied. Among the tested variables, four variables including TNZ solution pH, C_{TNZ}, dose of ZnO NPs and its calcination temperature were suggested by software as the most important influencing variables. Importance of calcination temperature can be related its important role on crystallite extent as well as phase purity and crystallite size of ZnO NPs, all are influencing factors that control its photo catalytic activity. Solution pH can control both surface charge of ZnO NPs and charges specieses of TNZ molecules in solution [44]. TNZ solution controls collision probability between TNZ molecules and OH radicals where produced at the catalyst surface as an important controlling factor for degradation extent of TNZ because OH radicals have a very short life time about a few nano-second [45]. Finally, dose

of ZnO NPs provides sufficient active sites for production of e/h pairs and finally OH and super oxide radicals as the main agents require for TNZ degradation.

Table 2 shows the actual and coded values of the most important influencing factors on the photo catalytic activity of ZnO-NPs in photo degradation of TNZ. Different factors involved in selected range for each variable. For example, selected pH range of 3–9 is based on pKa value of 3.1 for acidity of TNZ and pHpzc of ZnO NPs obtained at pH 7.8. A selected range for calcination temperature of ZnO NPs is based on the reported values in literature because it determines crystallite phase and purity of ZnO and also affects its crystallite size. In preliminary experiments, a 0.6 g/L of ZnO NPs showed a degradation extent of 54% for TNZ solution. Hence, a range was selected around this value.

For designing the experiments, the selected levels were inputted to design expert software. All suggested runs (30 runs including 6 center points for estimation of random errors) and the obtained degradation extents of CNZ after

Table 2
Coded and actual levels of the experimental variables

Factor	Name	Units	Low Actual	High Actual	Low Coded	High Coded	Mean
A	pH		3.10	9.00	−1	1	6.05
B	C_{TNZ}	ppm	2.50	5.50	−1	1	4.00
C	Ctal. Dos.	g/l	0.45	0.95	−1	1	0.70
D	Cal. Temp.	C	300.00	800.00	−1	1	550.00

performing the experiments based on the suggested conditions in each run are summarized in TSD1 (see supplementary data). As shown in TSD2, among the different models, the quadratic model was suggested for modeling the degradation process.

Hence, the following quadratic Eq. (1) was suggested by the model (β_0, β_i, β_{ii}, β_{ij} and ε are intercept or independent term, linear, squared, interaction coefficients and the experimental error, respectively) and after determination of the coefficient it was completed as Eq. (2).

$$Y = \beta_o + \Sigma\beta_i\, x_i + \Sigma\beta_{ii}\, x_i^2 + \Sigma\beta_{ij}x_ix_j + \varepsilon \tag{1}$$

$$\%D = 49.18 + 6.59\text{pH} - 24.50\ C_{TNZ} - 4.23\ \text{Dos} + 0.08\ \text{Tem}$$
$$+0.09\ \text{pH}{\times}C_{TNZ} - 0.04\ \text{pH} \times \text{Dos} + 6.91\text{E-}003\ \text{pH} \times \text{Tem} +$$
$$3.59\ C_{TNZ} \times \text{Dos} + 7.74\text{E-}003\ C_{TNZ} \times \text{Dos} + 0.06\ \text{Dos} \times \text{Tem} -$$
$$0.83(\text{pH})^2 + 1.88\ (C_{TNZ})^2 - 24.32(\text{Dos})^2 - 1.83\text{E-}004\ (\text{Tem})^2 \tag{2}$$

The residuals were normally distributed around the normal straight line. The plot of the studentized residuals versus runs and predicted one confirms the observed errors were normally distributed in ± 3σ confidence interval.

Some diagnostic plots including normal plot residuals, plot of residuals versus predicted and actual versus predicted are shown in FSD2, all confirm the goodness of the suggested model. In a well statistical model, residuals or random errors should be normally distributed. This can be shown by normal plot of residuals (or plot of normal probability % versus internally studentized residuals) (Fig. A in FSD2). As shown, a random distribution trend of residuals around the normal straight line is present, confirming a good model was suggested for the processing of data. Fig. FSD2B shows a plot of actual response values versus the predicted one. This plot helps us to detect a value (or group of values) that are not easily predicted by the model. As shown, the predicted responses by the model were well distributed around the actual responses. Plot of residuals versus predicted (the ascending predicted response values) measures the assumption of constant variance (FSD2-C). In this plot, generally, a random scatter is desired for the plot (constant range of residuals across the graph) and as shown here, the residuals were randomly distributed in the allowed range of ± 3. Well discussion on diagnostic and influencing plots is present in our previous work [46].

Based on the ANOVA (analysis of the variance) results in Table 3, the suggested model can well process the data obtained in the experiment for each suggested run. Here, F_{exp} for the model (28.76) is greater than its critical value of $F_{0.05,\,10,\,13} = 2.67$. This means that the significance of the suggested model at 95% confidence interval. A not significant lack of fit term (LOF, $F_{exp} = 2.4 < F_{0.05,\,13,\,3} = 8.73$) shows that replicate measurements on center points have good precision. LOF is a measure of random errors in the obtained data and evaluate the variation in the data around the fitted model. The F-value of 2.4 was obtained by dividing of mean square of the residual term to mean square of pure error term [46].

The R^2 values can also be sued for evaluation of the goodness of the model, so the values near the unit are better evidences for the goodness of regression of the data by the model (R^2 is 0.9687, Adj R^2 = 0.9350 and Pred. R^2 = 0.8626). On the other word, the predicted data suggested by the model and the obtained experimental data have good agreement and the model could well interpret the process. In addition, the values for adj-R^2 and R^2 are close that confirms all the selected variables have significant role in the response variable and the suggested model was not included by the non-significant terms [47,48].

The following formula was used for the Pareto analysis for showing the importance of each term in creation of the response.

$$P_i = \left(\frac{\beta_i^2}{\Sigma\beta_i^2}\right) \times 100\,(i \neq 0) \tag{3}$$

As shown in Fig. 5A, for the terms including the single factors TNZ concentration, solution pH and dose of the catalyst have 47.3, 3.4 and 1.4% importance, respectively. For the terms including interaction effects and quadratic factors, C_{TNZ}-Dose and Dose^2 have the most importance on creation of the response, respectively.

The best response was obtained in TNZ degradation in the run including pH 6.3, catalyst dosage 0.76 g L^{-1}, C_{TNZ} 2.5 mg L^{-1} for the ZnO calcined at 525°C. The applicability of the suggested model was evaluated by carrying out triplicate measurements in these conditions. The average degradation extent of 56.6% was obtained while the predicted value was 49.6 ± 4.2%. Hence, the predicted and experimental values have good agreement, confirming goodness of the model to modelize the process.

Interactions between calcination temperature and dose of the catalyst are shown by the corresponding 3D response surface in Fig. 5B. As shown, at the hole of the used dosage, the catalysts calcined at 400–600°C have the best activity in TNZ degradation. At lower calcination temperatures majority of ZnO NPs may be present as amorphous phase. At higher calcination temperatures above 600°C ZnO NPs may be aggregated, which significantly decreased the effective surface area and degradation efficiency.

Fig. 5C shows the simultaneous effects of solution pH and calcination temperature on the degradation extent of TNZ. As shown the best activities were obtained for the cat-

Table 3
ANOVA results obtained for the results

Source	Sum Sq.	d_f	Mean Sq.	F-Value	P-Value	
Block	979.94	2	489.97			
Model	7010.69	14	500.76	28.76	<0.0001	Significant
A: pH	106.98	1	106.98	6.14	0.0277	
B: C_{TNZ}	234.44	1	234.44	13.46	0.0028	
C: Catal. Dose	144.80	1	144.80	8.32	0.0128	
D: Cal. Temp.	13.91	1	13.91	0.80	0.03877	
AB	3.07	1	3.07	0.18	0.6814	
AC	0.015	1	0.015	8.618E-004	0.9770	
AD	415.85	1	415.85	23.88	0.0003	
BC	29.13	1	29.13	1.67	0.2184	
BD	134.85	1	134.85	7.74	0.0155	
CD	238.32	1	238.32	13.69	0.0027	
A^2	1430.26	1	1430.26	82.14	<0.0001	
B^2	491.09	1	491.09	28.20	0.0001	
C^2	63.36	1	63.36	3.64	0.0788	
D^2	3589.61	1	3589.61	206.14	<0.0001	
Residual	226.37	13	17.41			
Lack of Fit	201.21	10	20.12	2.40	0.2552	Not sig.
Puer Error	25.16	3	8.39			
Cor Total	8217.00	29				

alysts calcined at 400–600°C at pH range of 5–8. The pH_{pzc} for the catalyst was obtained at 7.8 based on the typical procedure illustrated in literature [49]. The catalyst surface has negatively and positively charged at pHs above and below of this value, respectively, while it has net zero charge at this pH. pKa value of TNZ is 3.1. Hence, at pHs below 3.1 majority of TNZ molecules may be present in the protonated form and repelled by the positively charged of ZnO surface at this pH. Similarly, the anionic/ or neutral forms of TNZ (due to presence of free electron pairs of nitrogen atoms) can be repelled by the negatively charged of ZnO surface at pHs > 8. In the pH range of 5–8, ZnO surface has net positive charge which attracts neutral TNZ molecules. Hence, degradation efficiency was increased.

3.4. Confirmation of TNZ degradation

To confirm the results obtained by UV-Vis spectra in photo degradation of TNZ, HPLC chromatograms of TNZ solution before and after photo degradation process were recorded and are shown in Fig. 6. As shown, the peak area of the main peak at retention time of 3.25 min was decreased after 90 photo degradation of sample. This corresponds to 62% degradation of TNZ molecules.
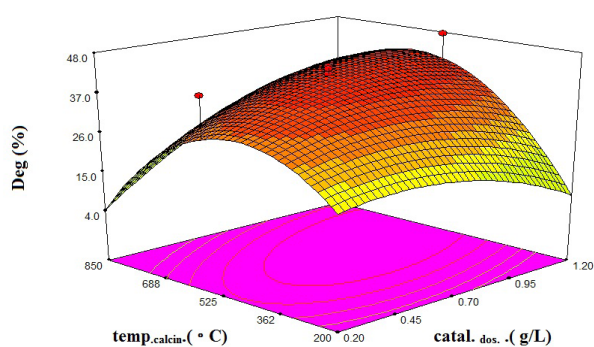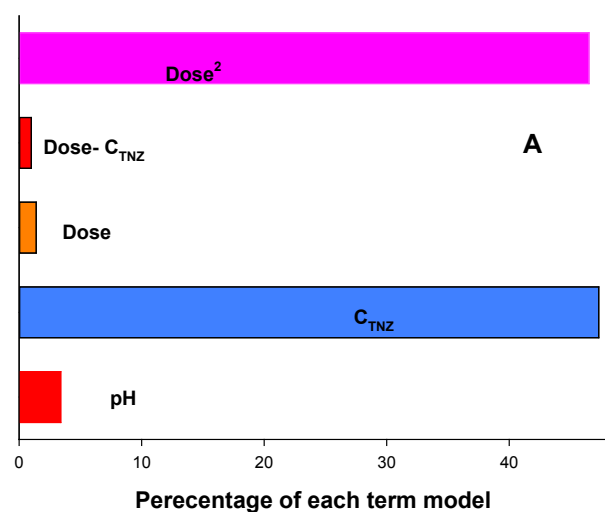
Also, COD (chemical oxygen demand) of TNZ was decreased from initial value of 980 mg/L to 288 mg/L after 90 min of photo degradation of solution (photo degradation conditions: C_{TNZ}: 2.5 mg/L at pH 6.3, 0.76 g/L of ZnO, irradiation time 90 min). This corresponds to 70% degradation of TNZ molecules. Hence, HPLC and COD results confirm degradation of TNZ molecules to smaller fragments during the photo degradation process.

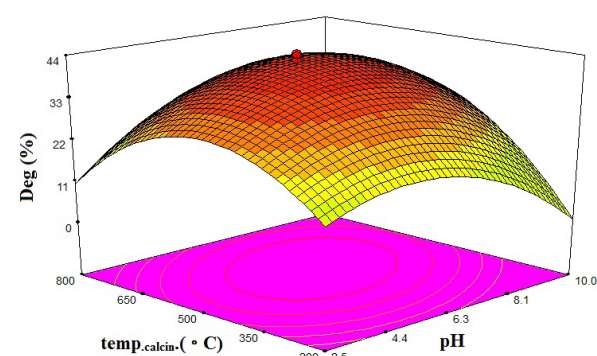### 3.5. Comparison of the work with other works

Based on our literature review, there are a few works on photo degradation of TNZ in aqueous solution. In a study, silica xerogels (XGS) have doped with different doses of Fe(III) by the sol-gel method and used in photo degradation of TNZ [50]. In our idea, the activity of this catalyst can be limited in pHs above 3 because in these pHs Fe(III) cations may be deactivated by hydrolysis process. In other work, UVC and solar lights assisted by H_2O_2, $K_2S_2O_8$ and photo-Fenton have used in photo degradation of TNZ [51]. The TNZ degradation percentage, its mineralization extent and its degradation products have been studied. The best results have been obtained in photo-Fenton process in the presence of both UV and solar lights. The used method is a homogeneous process which has some drawbacks such as pollution of water by secondary pollutants. In addition, Fenton process can be limited in activity at higher pHs. In the present work, a heterogeneous photo catalysis process was used and simultaneous interaction effects of the influencing variables were studied by experimental design.

4. Conclusions

In this work, ZnO nanoparticles (ZnO NPs) were synthesized in the presence of glycine as a stabilizing agent at pH 6. In this pH (iso-electric point of glycine), glycine present as di-pole ions as the predominant form in solution. It complexes Zn(II) cations from its negatively charged head, and its positively charged head repels the resulted complex species and prevents from their aggregation. Hence, conditions for production of nanoparticles was provided. Based

Fig. 6. HPLC chromatograms of TNZ solution before and after photo degradation process (C_{TNZ}: 2.5 mg/L at pH 6.3, 0.76 g/L of ZnO, irradiation time 90 min).

(B)

(C)

Fig. 5. A) Parreto plot for showing the importance of each term in the model; B-C) Some 3D response surfaces for showing the important interaction effects.

on RSM results, interaction effects of ZnO-dosage and calcination temperature caused the best photo catalytic activity thorough the used ZnO dosage in calcination temperature range of 400–600°C. This confirms that amorphous ZnO at lower calcination temperatures was formed that has little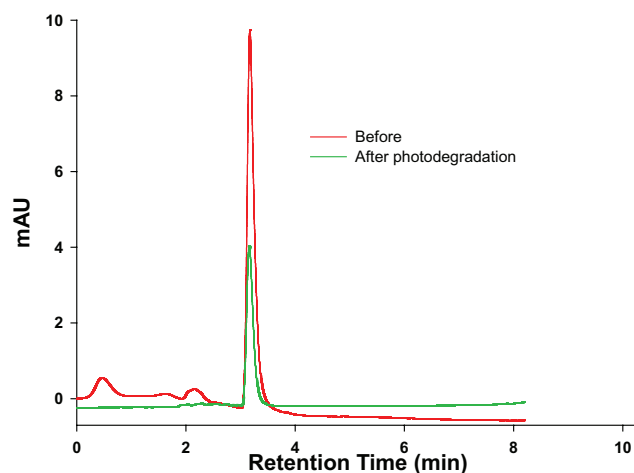 photo catalytic activity. In contrast,at higher calcination temperatures aggregation of ZnO NPs caused to decrease in its photo catalytic activity. The as synthesized ZnO NPs had pH_{pzc} of 7.8 and pKa value of TNZ is 3.1. In pH rang of 7–8 the best degradation extent was obtained, because in this pH range, neutral TNZ molecules can be adsorbed by positively charged ZnO surface.

References

[1] M. Yoosefian, S. Ahmadzadeh, M. Aghasi, M. Dolatabadi, Optimization of electro coagulation process for efficient removal of ciprofloxacin *antibiotic* using iron electrode; kinetic and isotherm studies of adsorption, J. Mol. Liq., 225 (2017) 544–553.

[2] M. Giahi, A.H. Dargahi, Photo catalytic degradation of phenylephrine hydrochloride in aqueous solutions by synthesized SnO_2-doped ZnO nano photo catalyst, Iran. J. Catal., 6(4) (2016) 381–387.

[3] P. Bansal, A. Verma, Pilot-scale single-step reactor combining photo catalysis and photo-Fenton aiming at faster removal of Cephalexin, J. Cleaner Prod., 195 (2018) 540–551.

[4] M. Carballa, F. Omil, J.M. Lema, M. Llompart, C. Garcia-Jares, I. Rodriguez, M. Gomez, T. Ternes, Behaviour of pharmaceuticals, cosmetics and hormones in a sewage treatment plant, Water Res., 38 (2004) 2918–2926.

[5] X.-l. Guo, Zh.-wei Zhu, H.-li Li, Biodegradation of sulfamethoxa zole by Phanerochaetechrysosporium, J. Mol. Liq., 198 (2014) 169–172.

[6] P. Raizada, J. Kumari, P. Shandilya, P. Singh, Kinetics of photo catalytic mineralization of oxytetracycline and ampicillin using activated carbon supported $ZnO/ZnWO_4$ nanocomposite in simulated wastewater, Desal. Water Treat., 79 (2017) 204–213.

[7] A. Buthiyappan, A.R. Abdul Aziz, W.M.A.W. Daud, Recent advances and prospects of catalytic advanced oxidation process in treating textile effluents, Rev. Chem. Eng., 32(1) (2016) 1–47.

[8] B.A. Ünnü, G. Gündüz, M. Dükkancı Heterogeneous Fenton-like oxidation of crystal violet using an iron loaded ZSM-5 zeolite, Desal. Water Treat., 57 (2016) 11835–11849.

[9] N. Masoudipour, M. Sadeghi, F. Mohammadi-Moghadam, Photo-catalytic inactivation of E. coli using stabilized Ag/S, N-TiO_2 nanoparticles by fixed bed photo-reactor under visible light and sunlight, Desal. Water Treat., 110 (2018) 109–116.

[10] H. Koohestani, S.K. Sadrnezha, Photo catalytic degradation of methyl orange and cyanide by using TiO$_2$/CuO composite, Desal. Water Treat., 57(46) (2016) 22029–22038.

[11] X. Lv, Y. Du, Z. Li, Z. Chen, K. Yang, T. Liu, C. Zhu, M. Du, Y. Feng, High photo catalytic property and crystal growth of spindle-like ZnO micro particles synthesized by one-step hydrothermal method, Vacuum, 144 (2017) 229–236.

[12] P. Nazari, F. Ansari, B.A. Nejand, V. Ahmadi, M. Payandeh, M. Salavati-Niasari, Physicochemical interface engineering of CuI/Cu as advanced potential hole-transporting materials/ metal contact couples in hysteresis-free ultra low-cost and large-area perovskite solar cells, J. Phys. Chem. C., 121(40) (2017) 21935–21944.

[13] M. Ghanbari, F. Ansari, M. Salavati-Niasari, Simple synthesis-controlled fabrication of thallium cadmium iodide nanostructures via a novel route and photo catalytic investigation in degradation of toxic dyes, Inorg. Chim. Acta, 455 (2017) 88–97.

[14] O. Amiri, N. Mir, F. Ansari, M. Salavati-Niasari, Design and fabrication of a high performance inorganic tandem solar cell with 11.5% conversion efficiency, Electrochim. Acta, 252 (2017) 315–321.

[15] F. Davar, M. Salavati-Niasari, Synthesis and characterization of spinel-type zinc aluminate nanoparticles by a modified sol–gel method using new precursor, J. Alloys Compd., 509 (2011) 2487–2492.

[16] O. Amiri, M. Salavati-Niasari, N. Mir, F. Beshkar, M. Saadat, F. Ansari. Plasmonic enhancement of dye-sensitized solar cells by using Au-decorated Ag dendrites as a morphology-engineered, Renew. Energy, 125 (2018) 590–598.

[17] F. Razi, F. Soofivand, M. Salavati-Niasari, Cu$_2$ZnI$_4$/ZnO nanocomposites: In-situ synthesis, characterization and optical properties, J. Mol. Liq., 222 (2016) 435–440.

[18] A. Nezamzadeh-Ejhieh, ZohrehBanan, Photodegradation of dimethyldisulfide by heterogeneous catalysis using nanoCdS and nanoCdO embedded on the zeolite A synthesized from waste porcelain, Desal. Water Treat., 52 (2014) 3328–3337.

[19] M. Karimi-Shamsabadi, M. Behpour, A. KazemiBabaheidari, Z. Saberi, Efficiently enhancing photo catalytic activity of NiO-ZnO doped onto nanozeoliteX by synergistic effects of p-n heterojunction, supporting and zeolite nanoparticles in photo-degradation of Eriochrome Black T and Methyl Orange, J. Photochem. Photobiol. A: Chem., 346 (2017) 133–143.

[20] M.M.J. Sadiq, A.S. Nesaraj, Reflux condensation synthesis and characterization of Co$_3$O$_4$ nanoparticles for photo catalytic applications, Iran. J. Catal., 4(4) (2014) 219–226.

[21] A. Elaziouti, N. Laouedj, B. Ahmed, ZnO-assisted photo catalytic degradation of congo red and benzopurpurine 4B in aqueous solution, J. Chem. Eng. Process Technol., 2 (2011) 1–9.

[22] A. Samad, M. Furukawa, H. Katsumata, T. Suzuki, S. Kaneco, Photo catalytic oxidation and simultaneous removal of arsenite with CuO/ZnO photo catalyst, J. Photochem. Photobiol. A: Chem., 325 (2016) 97–103.

[23] K.S. Ranjith, R.T. Rajendra Kumar, Surfactant free, simple, morphological and defect engineered ZnO nanocatalyst: Effective study on sunlight driven and reusable photo catalytic properties, J. Photochem. Photobiol. A: Chem., 329 (2016) 35–45.

[24] M. Masjedi-Arani, M. Salavati-Niasari, Metal (Mn, Co, Ni and Cu) doped ZnO-Zn$_2$SnO$_4$-SnO$_2$ nanocomposites: Green sol-gel synthesis, characterization and photo catalytic activity, J. Mol. Liq., 248 (2017) 197–204.

[25] N. Mir, M. Rakhshanipour, A. Heidari, A. Mir, M. Salavati-Niasari, Synthesis and characterization of ZnO nanohemispheres via solution-phase thermal decomposition and its comparison with the solid-phase approach, J. Ind. Eng. Chem., 21 (2015) 884–888.

[26] M. Salavati-Niasari, F. Davar, Z. Fereshteh, Synthesis and characterization of ZnO nanocrystals from thermolysis of new precursor, Chem. Eng. J., 146 (2009) 498–502.

[27] N. Mir, M. Salavati-Niasari, F. Davar, Preparation of ZnO nanoflowers and Zn glycerolate nanoplates using inorganic precursors via a convenient rout and application in dye sensitized solar cells, Chem. Eng. J., 181–182 (2012) 779–789.

[28] M. Salavati-Niasari, F. Davar, M. Mazaheri, Preparation of ZnO nanoparticles from [bis(acetylacetonato)zinc(II)]–oleyl-amine complex by thermal decomposition, Mater. Lett., 62 (2008) 1890–1892.

[29] F. Soofivand, M. Salavati-Niasari, F. Mohandes, Novel precursor-assisted synthesis and characterization of zinc oxide nanoparticles/nanofibers, Mater. Lett., 98 (2013) 55–58.

[30] M. Salavati-Niasari, N. Mir, F. Davar, ZnO nanotriangles: Synthesis, characterization and optical properties, J. Alloys Compd., 476 (2009) 908–912.

[31] M. Salavati-Niasari, F. Davar, A. Khansari, Nanosphericals and nanobundles of ZnO: Synthesis and characterization, J. Alloys Compd., 509 (2011) 61–65.

[32] B. Subash, B. Krishnakumar, M. Swaminathan, M. Shanthi, Synthesis and characterization of cerium–silver co-doped zinc oxide as a novel sunlight-driven photo catalyst for effective degradation of Reactive Red 120 dye, Mater. Sci. Semicond. Process, 16 (2013) 1070–1078.

[33] K. Ebel, H. Koehler, A.O. Gamer, R. Jäckh, Imidazole and Derivatives' In Ullmann's Encyclopedia of Industrial Chemistry; 2002 Wiley-VCH, doi:10.1002/14356007.a13-661.

[34] A. Asfaram, M. Ghaedi, Simultaneous determination of cationic dyes in water samples with dispersive liquid–liquid micro extraction followed by spectrophotometry: experimental design methodology, New J. Chem., 40 (2016) 4793–4802.

[35] B. ShayeghBoroujeny, N. Bazrafshan, Investigation of corrosion behavior of galvanized mild steel by improved Zn acidic bath containing ZnO nanoparticles, Adv. Mater. Process, 4 (2016) 3–11.

[36] S. Aghdasi, M. Shokri, Photo catalytic degradation of cipro floxacin in the presence of synthesized ZnO nanocatalyst: The effect of operational parameters, Iran. J. Catal., 6(5) (2016) 481–487.

[37] M. Mahdiani, F. Soofivand, F. Ansari, M. Salavati-Niasari, Grafting of CuFe$_{12}$O$_{19}$ nanoparticles on CNT and graphene: Eco-friendly synthesis, characterization and photo catalytic activity, J. Clean. Prod., 176 (2018) 1187–1195.

[38] F. Ansari, A. Sobhani, M. Salavati-Niasari, Simple sol-gel synthesis and characterization of new CoTiO$_3$/CoFe$_2$O$_4$ nanocomposite by using liquid glucose, maltose and starch as fuel, capping and reducing agents, J. Colloid Interf. Sci., 514 (2018) 723–732.

[39] M. Mahdiani, A. Sobhani, F. Ansari, M. Salavati-Niasari, Lead hexaferrite nanostructures: green amino acid sol–gel auto-combustion synthesis, characterization and considering magnetic property, J. Mater. Sci. Mater. Electron., 28 (2017) 17627–17634.

[40] A. Shokri, M.M. Ghazi, Preparation and characterizations of CuO doped ZnOnano-structure for the photo catalytic degradation of 4-chlorophenol under visible light, Adv. Environ. Technol., 1 (2016) 11–24.

[41] H.R. Pouretedal, M. Fallahgar, F.S. Pourhasan, M.Nasiri, Taguchi optimization of photo degradation of yellow water of trinitrotoluene production catalyzed by nanoparticles TiO$_2$/N under visible light, Iran. J. Catal., 7(4) (2017) 317–326.

[42] H. Derikvandi, A. Nezamzadeh-Ejhieh, Increased photo catalytic activity of NiO and ZnO in photo degradation of a model drug aqueous solution: Effect of coupling, supporting, particles size and calcination temperature, J. Hazard. Mater., 321 (2017) 629–638.

[43] S. Dianat, Visible light induced photo catalytic degradation of direct red 23 and direct brown 166 by InVO$_4$-TiO$_2$ nanocomposite, Iran. J. Catal., 8(2) (2018) 121–132.

[44] A. Eslami, A. Oghazyan, M. Sarafraz, Magnetically separable MgFe$_2$O$_4$ nanoparticle for efficient catalytic ozonation of organic pollutants, Iran. J. Catal., 8(2) (2018) 95–102.

[45] A. Nezamzadeh-Ejhieh, M. Khorsandi, Heterogeneous photo decolorization of Eriochrome Black T using Ni/P zeolite catalyst, Desalination, 262 (2010) 79–85.

[46] T. Tamiji, A. Nezamzadeh-Ejhieh, A comprehensive study on the kinetic aspects and experimental design for the voltammetric response of a Sn(IV)-clinoptilolite carbon paste electrode towards Hg(II), J. Electroanal. Chem. 829 (2018) 95–105.

[47] S.D. Khairnar, M.R. Patil, V.S. Shrivastava, Hydrothermally synthesized nanocrystalline Nb_2O_5 and its visible-light photo catalytic activity for the degradation of congo red and methylene blue, Iran. J. Catal., 8(2) (2018) 143–150.

[48] N. ElmiFarda, R. Fazaeli, Experimental design study of RB 255 photo catalytic degradation under visible light using synthetic Ag/TiO_2 nanoparticles: Optimization of experimental conditions, Iran. J. Catal., 8(2) (2018) 133–41.

[49] Z.-A. Mirian, A. Nezamzadeh-Ejhieh, Removal of phenol content of an industrial wastewater via a heterogeneous photo degradation process using supported FeO onto nanoparticles

of Iranian clinoptilolite, Desal. Water Treat., 57 (2016) 16483–16494.

[50] A. Acosta-Rangel, M. Sánchez-Polo, A.M.S. Polo, J. Rivera-Utrilla, M.S. Berber-Mendoza, Tinidazole degradation assisted by solar radiation and iron-doped silica xerogels, Chem. Eng. J., 344 (2018) 21–33.

[51] I. Velo-Gala, J.A. Pirán-Montaño, J. Rivera-Utrilla, M. Sánchez-PoloAntonio, J. Mota, Advanced oxidation processes based on the use of UVC and simulated solar radiation to remove the antibiotic tinidazole from water, Chem. Eng. J., 323 (2017) 605–617.
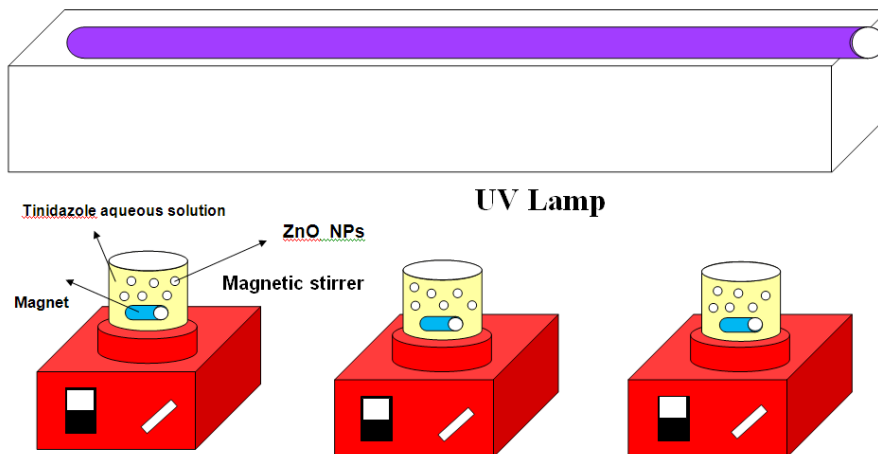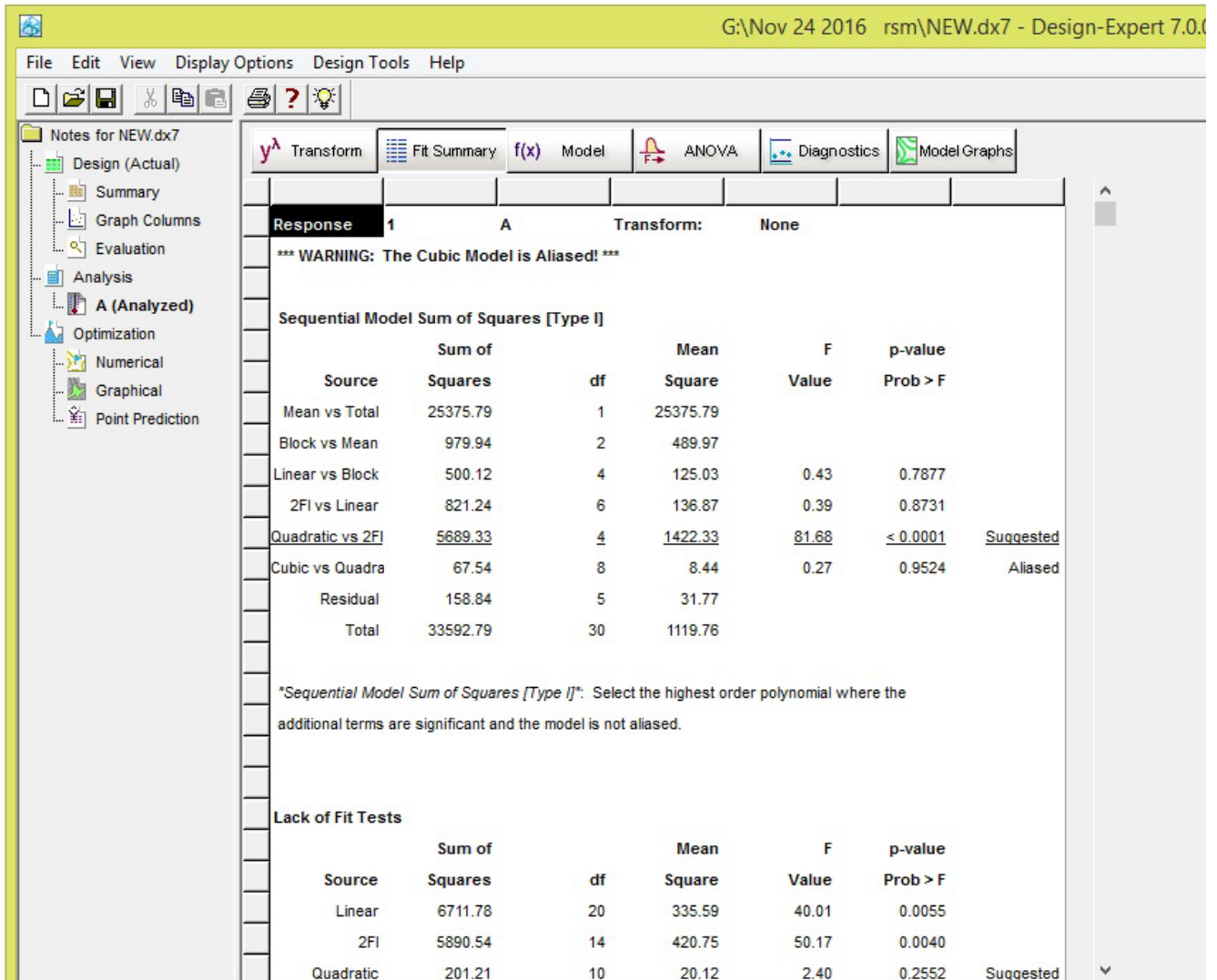
Supplementary Data

TSD1
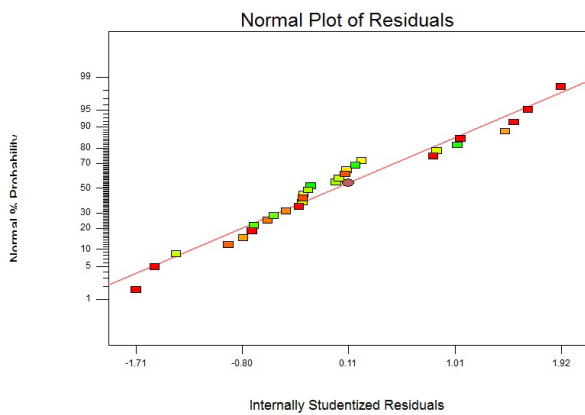The suggested run and response variable Y (D%) in TNZ degradation by ZnO-NPs.

Std	Run	Block	pH	C_{TNZ} (mg/L)	ZnO_{dose} g/L	Cal. Temp.°C	%D
12	1	Block 1	9.0	5.50	0.45	800	22.4
15	2	Block 1	3.1	5.50	0.95	800	23.3
8	3	Block 1	9.0	5.50	0.95	300	16.1
17	4	Block 1	6.1	4.00	0.7	550	43.9
5	5	Block 1	3.1	2.50	0.95	300	30.48
9	6	Block 1	3.1	2.50	0.45	800	10.0
2	7	Block 1	9.	2.50	0.45	300	28.2
18	8	Block 1	9.0	4.00	0.7	550	43
3	9	Block 1	6.1	5.50	0.45	300	21.9
14	10	Block 1	3.1	2.50	0.95	800	32.9
4	11	Block 2	9.0	5.50	0.45	300	11.00
7	12	Block 2	3.1	5.50	0.95	300	19.4
6	13	Block 2	9.0	2.50	0.95	300	19.9
1	14	Block 2	3.1	2.50	0.45	300	31.5
10	15	Block 2	9.0	2.50	0.45	800	17.9
20	16	Block 2	6.1	4.00	0.7	550	34.9
16	17	Block 2	9.0	5.50	0.95	800	34.5
11	18	Block 2	3.1	5.50	0.45	800	3.1
13	19	Block 2	3.1	2.50	0.95	800	17.8
19	20	Block 2	6.1	4.00	0.7	550	42.0
27	21	Block 3	6.1	4.00	0.7	50	5.8
25	22	Block 3	6.1	4.00	0.2	550	42.3
30	23	Block 3	6.1	4.00	0.7	550	43.4
23	24	Block 3	6.1	1.00	0.7	550	77.5
28	25	Block 3	6.1	4.00	0.7	1050	4.9
26	26	Block 3	6.1	4.00	1.2	550	47.6
29	27	Block 3	6.1	4.00	0.7	550	43.9
21	28	Block 3	0.2	4.00	0.7	550	15.9
24	29	Block 3	6.1	7.00	0.7	550	58.5
22	30	Block 3	12.0	4.00	0.7	550	28.5

TSD2
The statistical values obtained by RSM for the validation of the 'quadratic model' among all models

G:\Nov 24 2016 rsm\NEW.dx7 - Design-Expert 7.0.0							

File Edit View Display Options Design Tools Help

Notes for NEW.dx7
- Design (Actual)
  - Summary
  - Graph Columns
  - Evaluation
- Analysis
  - A (Analyzed)
- Optimization
  - Numerical
  - Graphical
  - Point Prediction

y^λ Transform   Fit Summary   f(x) Model   ANOVA   Diagnostics   Model Graphs

Response 1   A   **Transform:**   **None**

*** WARNING: The Cubic Model is Aliased! ***

Sequential Model Sum of Squares [Type I]

Source	Sum of Squares	df	Mean Square	F Value	p-value Prob > F	
Mean vs Total	25375.79	1	25375.79			
Block vs Mean	979.94	2	489.97			
Linear vs Block	500.12	4	125.03	0.43	0.7877	
2FI vs Linear	821.24	6	136.87	0.39	0.8731	
Quadratic vs 2FI	5689.33	4	1422.33	81.68	< 0.0001	Suggested
Cubic vs Quadra	67.54	8	8.44	0.27	0.9524	Aliased
Residual	158.84	5	31.77			
Total	33592.79	30	1119.76			

"Sequential Model Sum of Squares [Type I]": Select the highest order polynomial where the additional terms are significant and the model is not aliased.

Lack of Fit Tests

Source	Sum of Squares	df	Mean Square	F Value	p-value Prob > F	
Linear	6711.78	20	335.59	40.01	0.0055	
2FI	5890.54	14	420.75	50.17	0.0040	
Quadratic	201.21	10	20.12	2.40	0.2552	Suggested

UV Lamp

Tinidazole aqueous solution
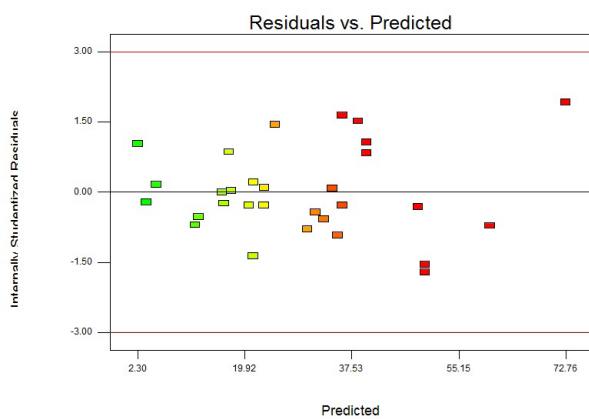
ZnO NPs

Magnetic stirrer

Magnet

FSD1. Schematic diagram for the used photo-reactor.

(A)
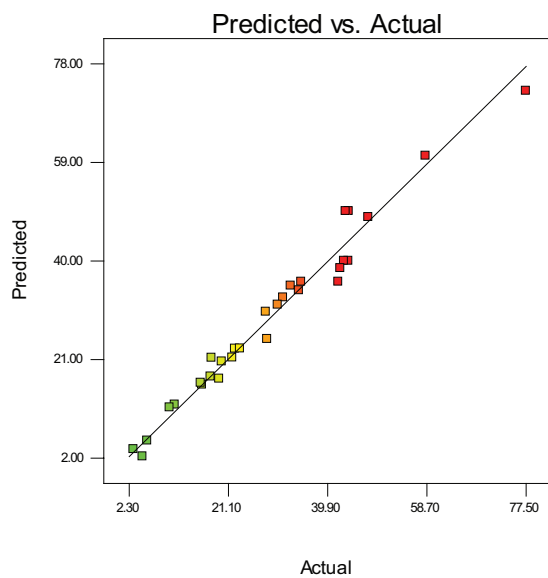
(B)

(C)

FSD2. (A) Normal probability plot of residuals, (B) Plot of actual vs predicted values in photo degradation of TNZ, (C) Plot of residuals versus model predicted values.